New Journal of Physics
The open access journal at the forefront of physics
Deutsche Physikalische Gesellschaft DPG | IOP Institute of Physics

H_2 and $(H_2)_2$ molecules with an *ab initio* optimization of wave functions in correlated state: electron–proton couplings and intermolecular microscopic parameters

Andrzej P Kądzielawa[1], Agata Bielas[2], Marcello Acquarone[3], Andrzej Biborski[4], Maciej M Maśka[2] and Józef Spałek[1,4]

[1] Instytut Fizyki im. Mariana Smoluchowskiego, Uniwersytet Jagielloski, ulica Łojasiewicza 11, PL-30348 Kraków, Poland
[2] Instytut Fizyki, Uniwersytet Śląski, ulica Uniwersytecka 4, PL-40007 Katowice, Poland
[3] Dipartimento di Fisica e Scienze della Terra dellUniversità di Parma, I-43100 Parma, Italy
[4] Akademickie Centrum Materiałów i Nanotechnologii, AGH Akademia Górniczo-Hutnicza, Aleja Mickiewicza 30, PL-30059 Kraków, Poland
E-mail: kadzielawa@th.if.uj.edu.pl and ufspalek@if.uj.edu.pl

Received 19 August 2014, revised 4 November 2014
Accepted for publication 12 November 2014
Published 8 December 2014

New Journal of Physics **16** (2014) 123022

doi:10.1088/1367-2630/16/12/123022

Abstract

The hydrogen molecules H_2 and $(H_2)_2$ are analyzed with electronic correlations taken into account between the $1s$ electrons in an exact manner. The optimal single-particle Slater orbitals are evaluated in the correlated state of H_2 by combining their variational determination with the diagonalization of the full Hamiltonian in the second-quantization language. All electron–ion coupling constants are determined explicitly and their relative importance is discussed. Sizable zero-point motion amplitude and the corresponding energy are then evaluated by taking into account the anharmonic contributions up to the ninth order in the relative displacement of the ions from their static equilibrium value. The applicability of the model to solid molecular hydrogen is briefly analyzed by calculating intermolecular microscopic parameters for the $2 \times H_2$ rectangular configuration, as well its ground state energy.

Keywords: hydrogen molecules, electron-proton coupling for hydrogen molecule, electronic correlations for hydrogen molecule, intermolecular hopping and interaction parameters

1. Motivation

The few-site models of correlated fermions play an important role in singling out, in an exact manner, the role of various local intra- and inter-site interactions against hopping (i.e., containing both covalent and the ionic factors) and thus, in establishing the optimal correlated state of fermions [1–8] on a local (nanoscopic) scale. The model has also been used to obtain a realistic analytic estimate of the hydrogen-molecule energies of the ground and the excited states in the correlated state [9]. For this purpose, we have developed the so-called EDABI method, which combines *E*xact *D*iagonalization in the Fock space with a concomitant *Ab I*nitio determination of the single-particle basis in the Hilbert space. So far, the method has been implemented by taking only 1*s* Slater orbitals, one per site [10]. The method contains no parameters; the only approximation made is taking a truncated single-particle basis (i.e., one Slater orbital per site) when constructing the field operator, that in turn is used to derive the starting Hamiltonian in the second-quantization representation. This Hamiltonian represents an extended Hubbard Hamiltonian, with *all* two-site interactions taken into account and the solution comprises not only the exact eigenvalues of the few-site Hamiltonian, but also at the same time an evaluation of the adjustable single-particle wave functions in the correlated state. Also, the calculated thermodynamic properties rigorously exemplify [12, 11] the low- and high-energy scales, corresponding to spin and local charge fluctuations, respectively. The former represents the precursory magnetic-ordering effect whereas the latter represents local effects accompanying the Mott–Hubbard transition. In general, our approach follows the tradition of accounting for interelectronic correlations via the second-quantization procedure, with the adjustment of single-particle wave functions, contained in microscopic parameters of the starting model, in the correlated state.

The first aim of this paper is to extend a previously established fully microscopic approach [9, 10] and calculate all six possible electron–ion coupling constants for H_2 as a function of the bond length. As a byproduct, we obtain an accurate estimate of the zero-point-motion amplitude and its energy to a high (ninth) order in the relative displacement of the ions. This evaluation shows explicitly the dominant contributions to the vibronic spectra of the molecule. In effect, the work formulates a complete two-site model of correlated states with all the coupling parameters calculated from an *ab initio* procedure. It also forms a starting point to full scale dynamic calculations involving a richer basis in the Hilbert space, at least in the adiabatic limit. So, although the importance of the present results to the discussion of the exact evaluation of the ground-state energy of the H_2 molecule is limited, the approach may be extended to treat molecular solid hydrogen with the inclusion of interelectronic correlations. Explicitly, as a starting point we calculate the intermolecular hopping integrals and the principal electron–electron interaction microscopic parameters as a function of intermolecular distance.

A methodological remark is in place here. As we determine the local ion–electron and electron–electron coupling parameters, they can be regarded as a starting estimate of those for the bulk solid molecular hydrogen, as we have recently studied a critical pressure of metallization of the *atomic* solid (Mott insulating) state [13]. The obtained pressure of atomic-

hydrogen metallization is about 100 GPa, a value which squares well with that observed for the case of fluid molecular hydrogen (140 GPa)[14], although the recent simulations provide quite different values for fluid hydrogen analyzed at high temperature [15]. Obviously, our previous work is not related directly to the molecular-hydrogen metallization in the solid state [16–19]. So far, we have discussed rigid-lattice properties. We believe that the present results form the first step in incorporating the vibrational spectrum and correlations to extended systems.

The structure of the paper is as follows. Even though the main purpose of the paper is to calculate the local electron–proton and electron–electron coupling constants, for the sake of the completeness, in sections 2 and 3 we reproduce some of the results of [9] and correct some minor errors (see also appendix A). In section 4 we define the method of calculation of both the electron–ion (proton) coupling constants (see also appendix B), as well as estimate the zero-point motion to the ninth order versus the interionic distance. In section 5 we extend the single-molecule treatment and provide the intermolecular hopping amplitudes and the electron–electron microscopic parameters which may serve for analysis of the solid molecular hydrogen. Section 6 contains physical discussion and a brief outlook, where we also refer to the finite-size quantum Monte Carlo results. In the series of appendices we provide some analytical details, as they may form an analytical basis for the electron–lattice coupling supplementing the classic Slater results for the electronic part of H_2 molecule [20].

2. Model and summary of purely electronic properties

2.1. Wannier basis

To describe the behavior of an electron in the system of two ions we start from $1s$ Slater–type orbitals

$$\Psi_i(\mathbf{r}) = \sqrt{\frac{\alpha^3}{\pi}}\, e^{-\alpha|\mathbf{r}-\mathbf{R_i}|}, \tag{1}$$

where α is the inverse size of the orbital. To ensure orthogonality we use Wannier functions, which in this case reduce the superposition of the atomic states, i.e.,

$$w_i(\mathbf{r}) = \beta\Big[\,\Psi_i(\mathbf{r}) - \gamma\Psi_j(\mathbf{r})\,\Big], \tag{2}$$

with the mixing parameters

$$\begin{cases} \beta = \dfrac{1}{\sqrt{2}}\sqrt{\dfrac{1+\sqrt{1-S^2}}{1-S^2}} \\ \gamma = \dfrac{S}{1+\sqrt{1-S^2}} \end{cases} \tag{3}$$

where $S = S(\alpha, R) \equiv \langle\Psi_1|\Psi_2\rangle$ is the atomic functions' overlap.

Equations (3) ensure both the orthogonality and proper behavior in the atomic limit i.e., $\lim_{R\to\infty}\beta = 1$, where R is the average interatomic distance. $\lim_{R\to\infty}\gamma = 0$.

2.2. Second-quantization picture

The two-site Hamiltonian with one orbital per site has the general form

$$\begin{aligned}\mathcal{H} = &\epsilon\left(\hat{n}_1 + \hat{n}_2\right) + t\sum_{\sigma}\left(\hat{a}^{\dagger}_{1\sigma}\hat{a}_{2\sigma} + \hat{a}^{\dagger}_{2\sigma}\hat{a}_{1\sigma}\right)\\ &+ U\left(\hat{n}_{1\uparrow}\hat{n}_{1\downarrow} + \hat{n}_{2\uparrow}\hat{n}_{2\downarrow}\right) - 2\,J\mathbf{S}_1\mathbf{S}_2\\ &+ \left(K - \frac{J}{2}\right)\hat{n}_1\hat{n}_2 + J\left(\hat{a}^{\dagger}_{1\uparrow}\hat{a}^{\dagger}_{1\downarrow}\hat{a}_{2\downarrow}\hat{a}_{2\uparrow} + h.\,c.\right)\\ &+ V\sum_{\sigma}\Big[\left(\hat{n}_{1\sigma} + \hat{n}_{2\sigma}\right)\left(\hat{a}^{\dagger}_{1\bar{\sigma}}\hat{a}_{2\bar{\sigma}} + \hat{a}^{\dagger}_{2\bar{\sigma}}\hat{a}_{1\bar{\sigma}}\right)\Big],\end{aligned} \tag{4}$$

where $\hat{a}_{i\sigma}$ and $\hat{a}^{\dagger}_{i\sigma}$ are the fermionic operators of annihilation and creation of the electron with spin σ on the $1s$ orbital of hydrogen atom $i \in \{1, 2\}$.

The microscopic parameters $\epsilon = T_{11}$, $t = T_{12}$, $U = V_{1111}$, $J = V_{1122}$, $K = V_{1212}$ and $V = V_{1112}$ correspond to one–and two-particle interactions [9]

$$T_{ij} = \left\langle w_i \left| \mathcal{T} \right| w_j \right\rangle, \tag{5a}$$

$$V_{ijkl} = \left\langle w_i w_j \left| \mathcal{V} \right| w_k w_l \right\rangle, \tag{5b}$$

where in atomic units $\mathcal{T} = -\nabla^2 - 2/|\mathbf{r} - \mathbf{R}|$, and $\mathcal{V} = 2/|\mathbf{r} - \mathbf{r}'|$. In appendix A we provide explicitly the form of microscopic parameters as a function of both intersite static distance R and the inverse wave-function size α. In what follows we first diagonalize (4), and subsequently optimize the wave functions contained in the microscopic parameters of (4). This program will be carried out systematically in what follows.

2.3. Exact solution

The system described by the Hamiltonian (4) has an exact solution previously studied in detail in [9]. For the two-electron system ($n_1 + n_2 = 2$), i.e. with one particle per site, the starting basis is

$$|1\rangle = \hat{a}^{\dagger}_{1\uparrow}\hat{a}^{\dagger}_{2\uparrow}|0\rangle, \tag{6a}$$

$$|2\rangle = \hat{a}^{\dagger}_{1\downarrow}\hat{a}^{\dagger}_{2\downarrow}|0\rangle, \tag{6b}$$

$$|3\rangle = \frac{1}{\sqrt{2}}\left(\hat{a}^{\dagger}_{1\uparrow}\hat{a}^{\dagger}_{2\downarrow} + \hat{a}^{\dagger}_{1\downarrow}\hat{a}^{\dagger}_{2\uparrow}\right)|0\rangle, \tag{6c}$$

representing the intersite spin-triplet states with eigenvalues $E_1 = E_2 = E_3 = 2\epsilon + K - J$, and

$$|4\rangle = \frac{1}{\sqrt{2}}\left(\hat{a}^{\dagger}_{1\uparrow}\hat{a}^{\dagger}_{2\downarrow} - \hat{a}^{\dagger}_{1\downarrow}\hat{a}^{\dagger}_{2\uparrow}\right)|0\rangle, \tag{6d}$$

$$|5\rangle = \frac{1}{\sqrt{2}}\left(\hat{a}^{\dagger}_{1\uparrow}\hat{a}^{\dagger}_{1\downarrow} + \hat{a}^{\dagger}_{2\uparrow}\hat{a}^{\dagger}_{2\downarrow}\right)|0\rangle, \tag{6e}$$

$$|6\rangle = \frac{1}{\sqrt{2}}\left(\hat{a}^{\dagger}_{1\uparrow}\hat{a}^{\dagger}_{1\downarrow} - \hat{a}^{\dagger}_{2\uparrow}\hat{a}^{\dagger}_{2\downarrow}\right)|0\rangle, \tag{6f}$$

representing the spin-singlet states, with the corresponding Hamiltonian matrix involving the matrix elements $\langle i\,|\mathcal{H}|\,j\rangle \equiv \left(\mathcal{H}_{ij}\right)$:

$$\left(\mathcal{H}_{ij}\right) = \begin{pmatrix} 2\epsilon + K + J & 2(t+V) & 0 \\ 2(t+V) & 2\epsilon + U + J & 0 \\ 0 & 0 & 2\epsilon + U - J \end{pmatrix}. \tag{7}$$

The state (6*f*) is an eigenvector of (7) with eigenvalue $E_6 = 2\epsilon + U - J$. The diagonalization supplies us with the two other eigenvectors [1]

$$|\pm\rangle = [2\mathcal{D}(\mathcal{D} \mp U \pm K)]^{-\frac{1}{2}} \\ [\mp(\mathcal{D} \mp U \pm K)|4\rangle + 4|t+V||5\rangle], \tag{8}$$

with eigenvalues

$$E_{\pm} = 2\epsilon + \frac{U+K}{2} + J \pm \frac{1}{2}\mathcal{D}, \tag{9}$$

where $\mathcal{D} = \sqrt{(U-K)^2 + 16(t+V)^2}$. The state $|-\rangle$ from (8) is the lowest-energy spin-singlet eigenstate. It is this state for which we determine explicitly the single-particle wave function and subsequently determine the microscopic parameters ϵ, t, U, J, K, and V explicitly, all as a function of interionic distance R.

2.4. Optimization of the atomic basis

The ground-state energy is the energy E_- of (9), supplemented with the ion–ion repulsion, i.e. by

$$E_G = E_- + \frac{2}{R}, \tag{10}$$

where $(2/R)$ is also represented in atomic units. As all the microscopic parameters are only a function of the distance R and the inverse wave-function size α, we have $E_G = E_G(\alpha, R)$. For each distance R, we minimize E_G with respect to α, thus closing the solution. Finally, we select $R = R_B$ as the equilibrium solution, for which the zero-point motion still has to be taken into account.

3. The stationary state for the H_2 molecule

In figure 1 we plot the energy of H_2 (dimer) versus the distance R. It is crucial that we obtain a local (and global) minimum at $R = R_B \equiv 0.757$ Å. This simple result obtained in [9] differs with respect to the virtually exact solution by Kołos and Wolniewicz [21, 22], $R_{K-W} = 0.74$ Å by 2.5% only.

In figure 2 we plot the sequence of the spin-singlets and the spin-triplet states. Parenthetically, the start from second-quantization language allows for evaluation of the ground-state and the lowest excited states, on an equal footing. This feature provides the difference with purely variational calculations in the first-quantization language. Namely,

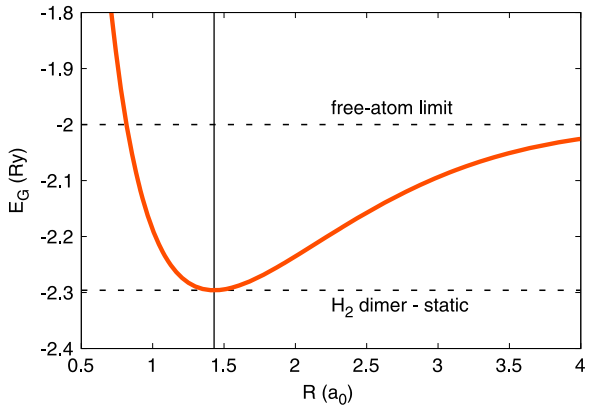

Figure 1. Ground-state energy—as defined by (10)—versus interionic static distance R. Note that the minimum value is $E_B = -2.295\,87\,Ry$ (marked by the vertical line here and below) at $R_B = 1.430\,42\,a_0$.

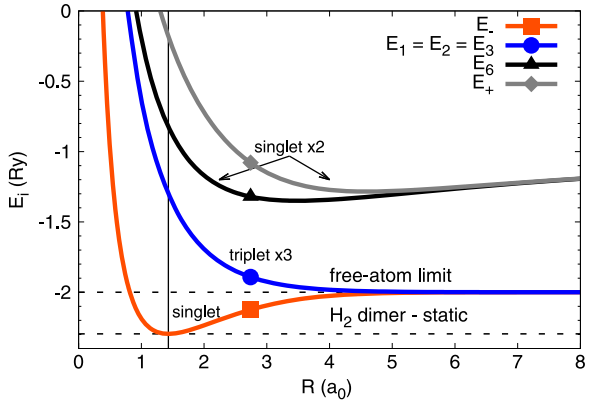

Figure 2. Solutions for the states: the spin-triplets ($E_1 = E_2 = E_3$) and the spin-singlets ($E_\pm$, E_6) versus the interionic distance R. The spin-singlet state $|-\rangle$ is the equilibrium state.

within this basis the spin-singlet state is stable at arbitrary interionic distance R. In figures 3–5 the inverse wave function size α, as well as all the microscopic parameters, are displayed as a function of the bond length R. One can see that with increasing R, the values tend to the proper free-atom limits. Those quantities form an input for the subsequent evaluation of electron–proton coupling constants discussed next.

4. Adiabatic approximation for the electron–ion coupling

Our principal aim here is to extend our previous model [9, 10] by allowing the ions to oscillate around the equilibrium positions. Thus the interionic distance R is taken now in the form

$$R = R_B + \delta R, \tag{11}$$

where δR is responsible for the zero-point motion. The electronic part of the ground-state energy is expanded next on δR in terms of a Taylor series, which to the ninth order reads

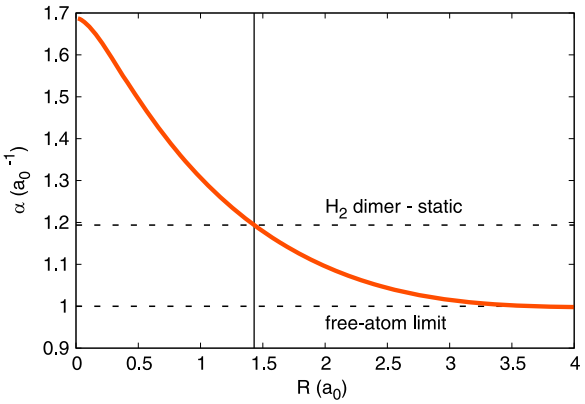

Figure 3. The optimal inverse wave-function size α versus the proton–proton average distance R. Note that $\alpha_B = 1.193\,78 a_0^{-1}$.

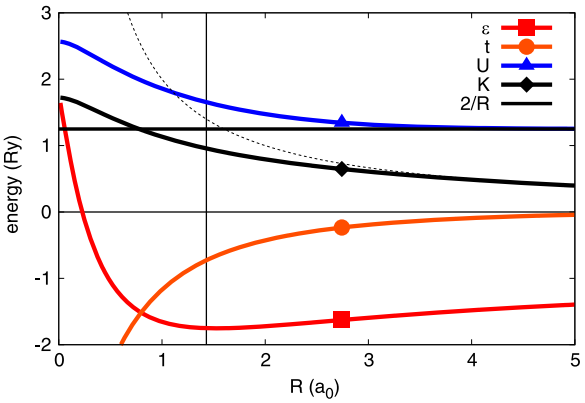

Figure 4. Microscopic parameters ϵ, t, U, and K versus average interionic distance R. Note the convergence of the intersite Coulomb repulsion K to the classical value $2/R$ (dashed line) at $R \to \infty$. The on-site repulsion U also reaches its atomic limit $U_{at} = 1.25\,Ry$, whereas the hopping parameter $t \to 0$.

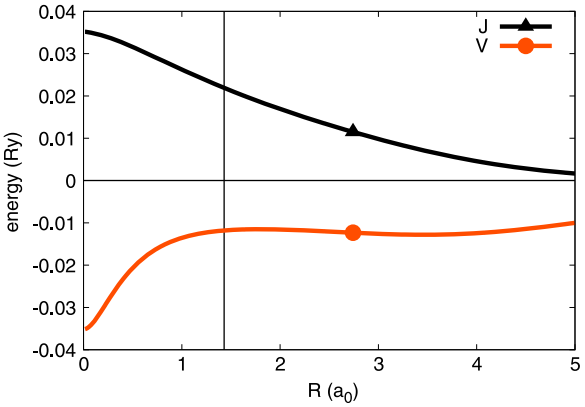

Figure 5. Microscopic parameters J and V versus R. Note that the exchange integral is always ferromagnetic, and the so-called correlated hopping parameter is $V < 0$.

$$\langle \mathcal{H} \rangle_{\delta R} = E_B + \sum_{i=2}^{9} \frac{1}{i!} E_B^{(i)} \delta R^i + O\left(\delta R^{10}\right), \tag{12}$$

where $E_B^{(i)} = \left.\frac{\partial^i E_B}{\partial R^i}\right|_{R_B}$ and $E_B^{(1)} = 0$, whereas all the remaining terms but for the energy E_B describe the oscillations (see table 2 for numerical values). We have modified the Hamiltonian (4) accordingly by taking into account δR, i.e.,

$$\mathcal{H} \to \mathcal{H} + \delta\mathcal{H}, \tag{13}$$

where $\delta\mathcal{H}$ is the additional term. Also, $\mathcal{H}$ simplifies to the form

$$\mathcal{H} = \sum_i \Xi_i \hat{O}_i, \tag{14}$$

where $\Xi = \{\epsilon, t, U, J, K, V\}$ and $\hat{O}_i$ are the corresponding operator parts of Hamiltonian: the two- and four-operator terms of (4) standing next to the respective microscopic parameter (for example $\hat{O}_\epsilon = \hat{n}_1 + \hat{n}_2$). With the Hamiltonian in this form we now have the energy change due to the change of the microscopic parameters

$$\delta\mathcal{H} = \sum_i \delta\Xi_i \hat{O}_i = \sum_i \xi_i \delta R\ \hat{O}_i, \tag{15}$$

where $\xi_i \equiv \frac{\delta \Xi_i}{\delta R}$. Since $\delta R \propto (b_i^\dagger + b_i)$, where $b_i^\dagger$, b_i are bosonic creation and annihilation operators of the system deformation and the set $\{\xi_i\}$ defines a new set of microscopic parameters—the electron–ion coupling constants. They can be derived by differentiation in a way similar to that of [23, 24] (see appendix B for details).

The shift of the ions changes the system properties in the following manner

$$\langle \delta\mathcal{H} \rangle = \sum_i \xi_i \left\langle \hat{O}_i \right\rangle_0 \delta R, \tag{16}$$

where the average $\langle \hat{O}_i \rangle_0 = \langle - \left| \hat{O}_i \right| - \rangle$ is taken with respect to the ground state. In effect, we obtain

$$\left\langle \hat{O}_\epsilon \right\rangle_0 = 2, \tag{17a}$$

$$\left\langle \hat{O}_t \right\rangle_0 = \frac{8|t+V|}{\mathcal{D}}, \tag{17b}$$

$$\left\langle \hat{O}_U \right\rangle_0 = \frac{16(t+V)^2}{2\mathcal{D}(\mathcal{D}+U-K)}, \tag{17c}$$

$$\left\langle \hat{O}_J \right\rangle_0 = 1, \tag{17d}$$

$$\left\langle \hat{O}_K \right\rangle_0 = \frac{\mathcal{D}+U-K}{2\mathcal{D}}, \tag{17e}$$

$$\left\langle \hat{O}_V \right\rangle_0 = \frac{8|t+V|}{\mathcal{D}}. \tag{17f}$$

The R dependence of the parameters $\langle \hat{O}_i \rangle$ given by (17) is displayed in figure 6. As they are of the order of unity, the principal factor determining the relative strength of the coupling

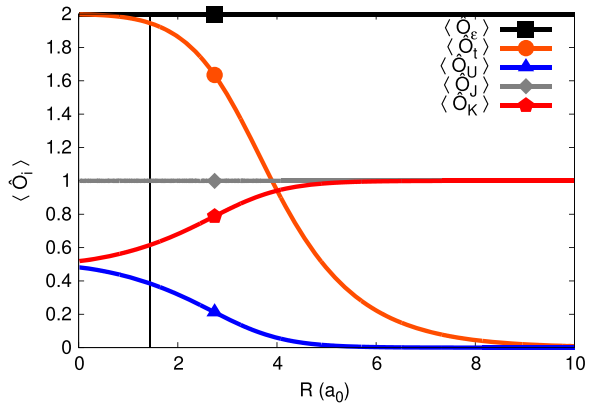

Figure 6. Averages (17) calculated in the ground-state versus distance R. They are of the order of unity.

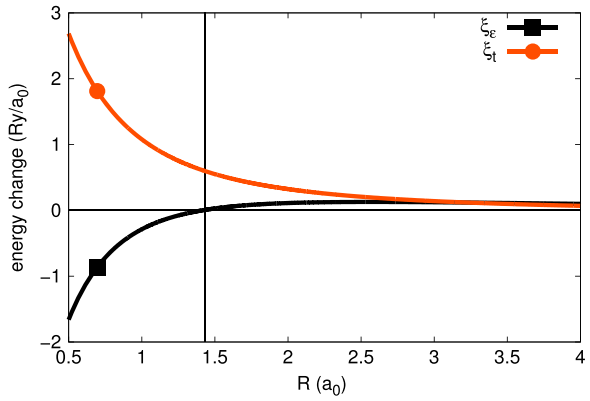

Figure 7. Coupling constants ξ_ϵ and ξ_t versus intersite distance R.

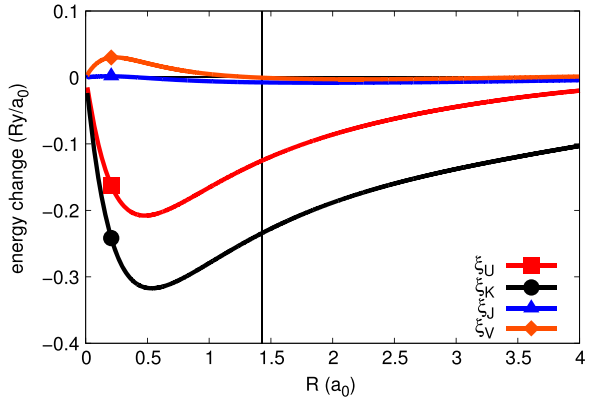

Figure 8. Coupling constants ξ_U, ξ_K, ξ_J and ξ_V versus intersite distance R

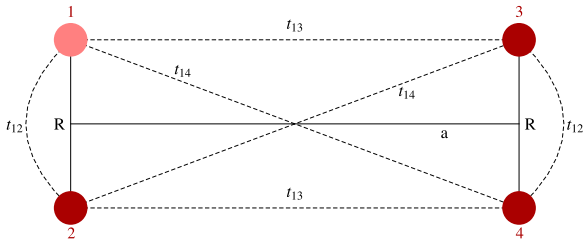

Figure 9. The system of two H_2 molecules at the relative distance a. The hopping integrals t_i are marked next to the respective dashed lines. Note that the orthogonalization procedure for four sites produces a different basis than that obtained in (3).

constants is provided by the parameters $\{\xi_i\}$ displayed in figures 7 and 8. At the equilibrium bond distance marked by the vertical line, the largest values are (on the absolute scale) those coming from modulation of the hopping parameter (ξ_t) and the change of intersite Coulomb interaction (ξ_K). The first of the two has been included in the Su, Schrieffer and Heeger model [25]. The second may play an important role in the high-T_C superconductivity [24]. Also, we see that the so-called Holstein coupling [26] is not important if calculated near the hydrogen-molecule equilibrium state.

We determine the value of δR by minimizing the total energy of the system:

$$E_{\text{total}} \equiv \langle \mathcal{H} \rangle + \langle \delta \mathcal{H} \rangle + \left\langle \mathcal{H}_{\text{ion}} \right\rangle. \tag{18}$$

where

$$\left\langle \mathcal{H}_{\text{ion}} \right\rangle = 2\frac{\delta P^2}{2\,M} + \frac{2}{R + \delta R}. \tag{19}$$

where the ionic momentum δP is evaluated via the Heisenberg principle and $M \overset{a.u.}{\approx} 1836.152\,67$ is the mass of the proton.

5. Evaluation of the microscopic parameters for the two-molecule system

We extend our approach by considering a system of two H_2 dimers at a relative distance a from each other (see figure 9). We calculate the respective hopping integrals, where t_{12} should approach t defined in (A.1*b*) for large a, and the new single-particle energy ϵ should again converge to previously obtained value (A.1*a*). We determine all the two-particle interaction integrals, thus going beyond the Hubbard model solved in [5]. Additionally, in table 1 we list the numerical values of the most relevant microscopic parameters.

The results are presented in figures 10–13. Note that all the results converge to the free-molecule ($a \to \infty$) values. The calculated hopping values of t_{13} and t_{14} may serve as input parameters for H_2 molecular crystal.

Explicitly, in figure 10 we display the intermolecular dependence of single-particle parameters. For the distances $a \gtrsim 2\,a_0$ the hoppings t_{13} and t_{14} can be regarded as small on the scale $t_{12} = t$. Hence, the system in a solid will preserve its molecular character, with no magnetism involved even though we have nominally one electron per atom. In other words, the lowest band will be full and no simple-minded Hubbard subband (HOMO-LUMO) picture in the ground state appears. In figure 11 we compare the relative values of intramolecular (U,

Table 1. Numerical values of single-particle energy (ϵ), the hopping integrals ($t_{\alpha\beta}$), the on-site Coulomb repulsion U and the intramolecular Coulomb interaction K_{12} for the two-molecule system; values refer to the points marked in the figure 13.

R (a_0)	a (a_0)	ϵ (Ry)	t_{12} (Ry)	t_{13} (Ry)	t_{14} (Ry)	U (Ry)	K_{12} (Ry)	K_{13} (Ry)	K_{14} (Ry)
0.715	1.43	−3.4265	−1.5534	−0.9320	0.2799	1.9210	1.2082	1.0480	0.8405
0.715	2.86	−2.9068	−1.3948	−0.2349	0.0993	1.7875	1.1386	0.6790	0.5976
0.715	4.29	−2.5229	−1.3671	−0.0499	0.0339	1.7557	1.1233	0.4674	0.4369
1.43	1.43	−3.4500	−0.8030	−0.8030	0.1023	1.8143	1.0127	1.0127	0.7514
1.43	2.86	−3.0007	−0.7504	−0.2232	0.0279	1.6903	0.9699	0.6732	0.5655
1.43	4.29	−2.6483	−0.7380	−0.0535	0.0096	1.6585	0.9587	0.4666	0.4245
2.145	1.43	−3.2344	−0.4278	−0.7651	0.0500	1.7359	0.8269	0.9858	0.6552
2.145	2.86	−2.8805	−0.4211	−0.2294	0.0013	1.6162	0.8047	0.6674	0.5223
2.145	4.29	−2.5668	−0.4185	−0.0610	−0.0019	1.5839	0.7977	0.4655	0.4056
2.86	1.43	−3.0007	−0.2232	−0.7504	0.0279	1.6903	0.6732	0.9699	0.5655
2.86	2.86	−2.7193	−0.2354	−0.2354	−0.0075	1.5712	0.6631	0.6631	0.4739
2.86	4.29	−2.4410	−0.2385	−0.0670	−0.0066	1.5383	0.6593	0.4646	0.3816

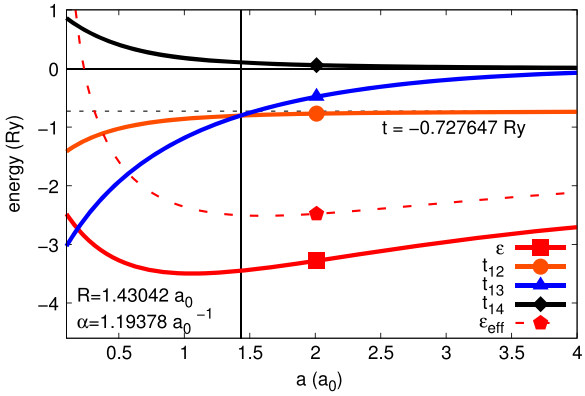

Figure 10. The one-particle microscopic parameters for two H_2 molecules system versus intermolecular distance a. The red dashed line marks the effective (renormalized by ion–ion repulsion) single-particle energy per site $\epsilon_{\text{eff}} = \epsilon + 1/N \sum_i 2/R_i$. Note the convergence of $t_{12} \to t$, and t_{13}, $t_{14} \to 0$ with $a \to \infty$. The equality of t_{12} and t_{13} at $a = R_B = 1.430\,42\ a_0$ should be observed as well.

Table 2. The numerical values of coefficients in Taylor series of ground-state energy. Up to the term $E_B^{(6)}$ all of the derivatives are calculated analytically from equation (10). Orders seventh–ninth (marked by an asterisk) were calculated numerically due to complicated analytical expression for ground-state energy.

$E_B^{(1)}\left(\frac{Ry}{a_0}\right)$	0.0
$\frac{1}{2!}E_B^{(2)}\left(\frac{Ry}{a_0^2}\right)$	0.430 045
$\frac{1}{3!}E_B^{(3)}\left(\frac{Ry}{a_0^3}\right)$	−0.464 021
$\frac{1}{4!}E_B^{(4)}\left(\frac{Ry}{a_0^4}\right)$	0.354 584
$\frac{1}{5!}E_B^{(5)}\left(\frac{Ry}{a_0^5}\right)$	−0.253 393
$\frac{1}{6!}E_B^{(6)}\left(\frac{Ry}{a_0^6}\right)$	0.174 863
$\frac{1}{7!}E_B^{(7)}\left(\frac{Ry}{a_0^7}\right)^*$	−0.119 178
$\frac{1}{8!}E_B^{(8)}\left(\frac{Ry}{a_0^8}\right)^*$	0.081 758 6
$\frac{1}{9!}E_B^{(9)}\left(\frac{Ry}{a_0^9}\right)^*$	−0.056 383 7

$K_{12} = K$) versus intermolecular (K_{13}, K_{14}) Coulomb interactions. Again, intramolecular interactions dominate for $a \gtrsim 2\ a_0$. From figures 10 and 11 it follows then that in the insulating (molecular-crystal) state, virtual hopping processes will contribute and renormalize the gap between the full-band (valence) and the conduction-band (excited single electron) states in a similar manner to the kinetic exchange. This gap will have the form of the Hubbard gap, as the value of U, corresponding to the transition $2H_2 \to H_2^- + H_2^+$ will have the value

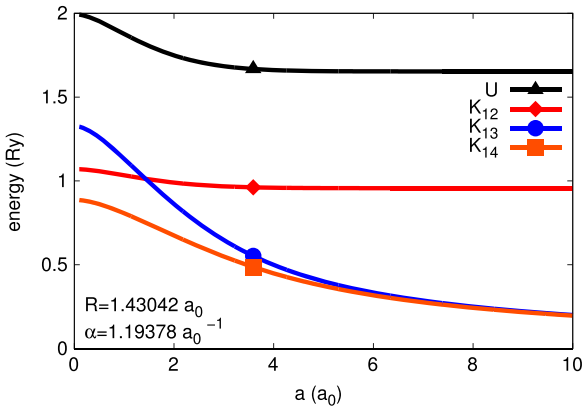

Figure 11. Coulomb-interaction microscopic parameters: the on-site part (U), intramolecular (K_{12}), and intermolecular K_{13} and K_{14} for two H_2-molecule system versus intermolecular distance a.

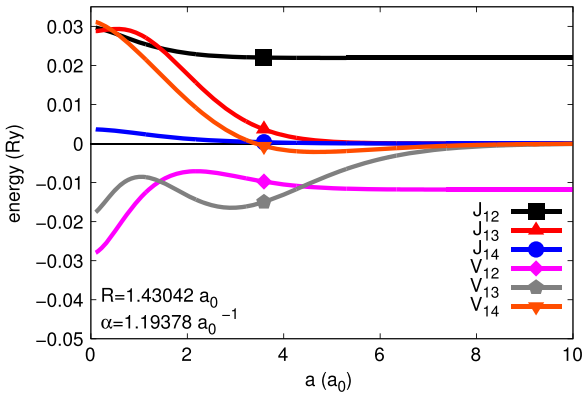

Figure 12. Two-particle microscopic parameters: intramolecular spin-exchange J_{12} and correlated hopping V_{12}, as well as the intermolecular parameters J_{13}, J_{14}, V_{13} and V_{14} for two H_2 molecules system versus intermolecular distance a. Note that all the intermolecular parameters converge to zero quickly.

$U - K_{12} \approx 0.6\,Ry$, by far the largest energy in the insulating state. For the sake of completeness, we have plotted in figure 12 the remaining interaction parameters: the exchange integrals, intra- (J_{12}) and inter-molecular (J_{13} and J_{14}), as well as the correlated hopping amplitudes: V_{12} and (V_{13} and V_{14}), respectively.

In figure 14 we show the difference between the energies of the $\left(H_2\right)_2$ system and that of the free molecules (per molecule):

$$\Delta E_{H_2} = \frac{E_{(H_2)_2}}{2} - E_B, \tag{20}$$

where $E_{(H_2)_2}$ is the energy of the $\left(H_2\right)_2$ system and $E_B = -2.295\,87\,Ry$ is the energy of single molecule. The equilibrium parameters are $\Delta E_{H_2} = -0.011\,29\,Ry$ and $a = 4.5a_0$. Those results are in agreement with the earlier estimates [28]. The stability of hydrogen molecular clusters were also studied in [29, 30]; our approach coherently incorporates electronic correlations (a

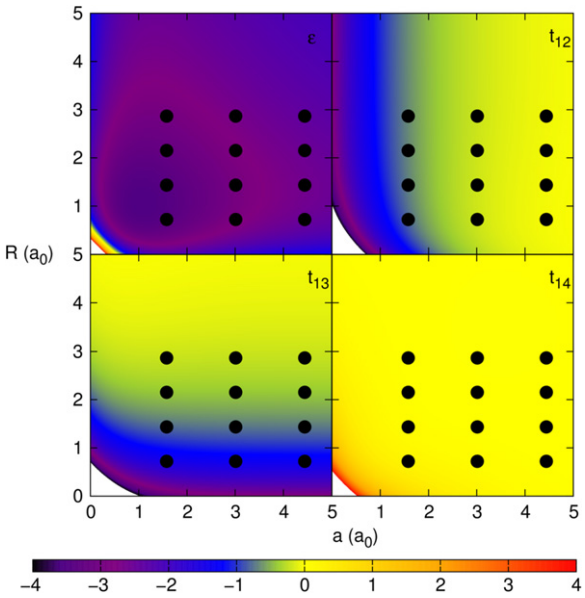

Figure 13. The one-particle microscopic parameters (in Ry) for the two H_2 molecule system versus intermolecular distance a and interionic distance R. Note the symmetry of ϵ and t_{14}. As expected for relatively small distances, values of t_{12} and t_{13} are negative whereas t_{14} is positive. When approaching point (0, 0) all parameters diverge to negative (t_{12} and t_{13}) or positive (ϵ and t_{14}) infinity. The explicit values of the marked points are given in table 1

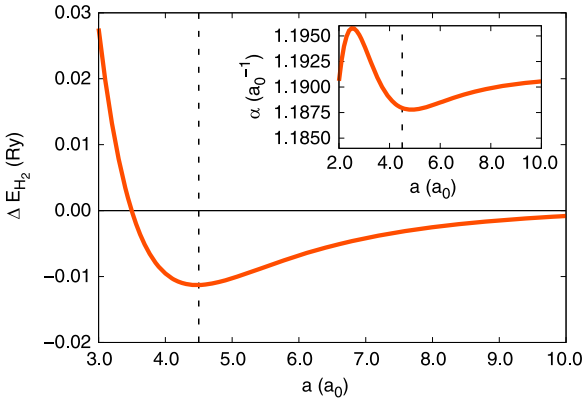

Figure 14. Difference between the energies of the $\left(H_2\right)_2$ system and that of the free molecules (per molecule) versus intermolecular distance a. Note the van der Waals-like behavior with the shallow minimum at $a = 4.5\, a_0$. Inset: inverse atomic wave-function size α versus a. For $a \to \infty$, it approaches the value $\alpha_B = 1.193\,78\, a_0^{-1}$. The behavior is similar to the one in [27].

necessity in describing the non-polar systems) into the molecular picture, which plays an important role in view of the existence of the minima of the $\Delta E_{H_2}(a)$ curve [28, 29].

Table 3. The values (in atomic units) of the microscopic parameters of Hamiltonian (4) and the electron–ion coupling constants from (15) at the hydrogen-molecule equilibrium ($R = R_B$ and $\alpha = \alpha_B$).

microscopic paramters (Ry)		coupling constants (Ry/a_0)	
ϵ	−1.750 79	ξ_ϵ	0.006 161 65
t	−0.727 647	ξ_t	0.598 662
U	1.653 21	ξ_U	−0.124 934
K	0.956 691	ξ_K	−0.234 075
J	0.021 9085	ξ_J	−0.007 463 03
V	−0.011 7991	ξ_V	−0.000 426 452

6. Discussion of results and outlook

The evaluation of the global parameters of the system can be summarized as follows:

1. The H_2 binding energy is $E_B = -2.295\,87Ry$. This value can be compared to the Kołos-Wolniewicz value [21]: $E_{\mathrm{K-W}} = -2.349\,Ry$, which is about 2.26% lower than the value obtained here.
2. The increase of the binding energy here is due to the zero-point motion, which is

$$E_{ZPM} = 0.024\,072Ry, \tag{21}$$

   and is of the order 1.0485% of the binding energy.
3. Whereas the bond length is here $R_B = 1.430\,42\,a_0$ (as compared to $R_{\mathrm{K-W}} = 1.3984\,a_0$, which is 2.29% lower), the zero-point motion amplitude is $|\delta\mathbf{R}| = 0.189\,028\,a_0$, a rather large value. Note that the optimal size of the inverse orbit of the $1s$ component hydrogen orbital is $\alpha_B = 1.193\,78\,a_0^{-1}$, so that the effective Bohr orbit is $a \equiv \alpha^{-1} = 0.8377\,a_0$. The Bohr orbit decrease is due to the increased binding of electron in the molecule $\sim$0.2932 Ry with respect to that in the hydrogen atom. The size a is substantially smaller than that of $1s$ orbit (1.06 Å) in H atom [9].
4. The ion–electron coupling constants versus R are shown in figures 7 and 8, whereas their values for $R = R_B$ are listed in table 3. We also provide the second-order coupling constants values at the hydrogen-molecule equilibrium in table 4. Our first-principle calculations allow us to claim that the coupling constant appearing in the Holstein model [26] (ξ_ϵ) is decisively smaller than those of the Su, Schrieffer and Heeger model [25] (ξ_t) as well as of those coming from the intersite direct Coulomb interaction (ξ_K). This should not be surprising, as the dominant coupling parameters represent interatomic-vibration contributions. A separate branch is represented by phonon excitations, but their analysis requires a construction of a spatially extended system of the molecules.

The question is to what extent the calculated local characteristics will represent their local counterparts in the molecular-solid phase. Certainly, the phonons and the molecule-rotational degrees of freedom will represent low-energy excitations. But the zero-point motion energy of

Table 4. The values (in atomic units) of the second-order electron–ion coupling constants $\xi_i^2 = \delta^2\Xi/\delta R^2$ at the hydrogen-molecule equilibrium ($R = R_B$ and $\alpha = \alpha_B$).

coupling constants (Ry/a_0^2)	
ξ_ϵ^2	0.327 335
ξ_t^2	−0.560 426
ξ_U^2	0.050 4027
ξ_K^2	0.013 028
ξ_J^2	−0.006 715 66
ξ_V^2	−0.010 5204

the whole molecule should have to be added. Will this provide a reliable description of the molecular or atomic hydrogen even though our accuracy in determining the individual-molecule energy is about 2% higher than the virtually exact value of Kołos and Wolniewicz [21]? One has to check and this task is under consideration in our group. Such consideration must include the inter-molecular hopping integrals t_{13} and t_{14}. One should also note that the proper method of treating the few-site H_2-molecule system is the quantum-Monte-Carlo-method [31–33]. Nonetheless, our method evaluates both the system energetics and the wave-function renormalization at the same time in the correlated state.

One can also extend the present model of the molecular binding by also including $2s$ and $2p$ adjustable hydrogen orbitals in the Hilbert space of the single-particle states via the corresponding Gaussian representation. The first estimate of the $2s$-orbital contribution to selected microscopic parameters is briefly discussed in appendix D. Their numerical values are provided in 6. One can see that the basis extension leads to the numerically relevant corrections. This is an additional route to follow, but only after the first-principle calculations of the solid phase along the lines discussed here is undertaken and tested.

Very recently [34], the dynamical mean field theory (DMFT) has been applied to the H_2 molecule and its accuracy tested. Our approach in this respect is much simpler, but still provides comparable accuracy. Also, we have calculated the vibronic coupling constants, which have been determined accurately recently [35]. Those results compare well with our estimates. This circumstance shows again that our method forms a proper starting point for treatment of solid molecular hydrogen, as a correlated state, at least in the insulating phase.

Acknowledgments

The authors (APK & JS) are grateful the Foundation for Polish Science (FNP) for financial support within the TEAM Project. MA is grateful to the Jagiellonian University for hospitality and FNP for a partial support for his visit. JS is grateful to the National Science Center (NCN) for the support within the MAESTRO project, grant no. DEC-2012/04/A/ST3/00342. APK's visit to the University of Parma has been financially supported by the grant of the Polish Ministry of Science and Higher Education, grant no. 7150/E-338/M/2013. MMM acknowledges support by the Polish National Science Center (NCN) under grant no. DEC-2013/11/B/ST3/00824.

Appendix A. Exact solution without the zero-point motion

For the sake of completeness we express the microscopic parameters defined in (5) in terms of *single-particle parameters* via (2)

$$\epsilon = \beta^2\left(1+\gamma^2\right)\epsilon' - 2\beta^2\gamma t', \tag{A.1a}$$

$$t = \beta^2\left(1+\gamma^2\right)t' - 2\beta^2\gamma\epsilon', \tag{A.1b}$$

$$U = \beta^4\Big[\left(1+\gamma^4\right)U' + 2\gamma^2K' - 4\gamma\left(1+\gamma^2\right)V' + 4\gamma^2J'\Big], \tag{A.1c}$$

$$K = \beta^4\Big[2\gamma^2U' + \left(1+\gamma^4\right)K' - 4\gamma\left(1+\gamma^2\right)V' + 4\gamma^2J'\Big], \tag{A.1d}$$

$$J = \beta^4\Big[2\gamma^2U' + 2\gamma^2K' - 4\gamma\left(1+\gamma^2\right)V' + \left(1+\gamma^2\right)^2J'\Big], \tag{A.1e}$$

$$V = \beta^4\Big[-\gamma\left(1+\gamma^2\right)U' - \gamma\left(1+\gamma^2\right)K' + \left(1+6\gamma^2+\gamma^4\right)V' - 2\gamma\left(1+\gamma^2\right)J'\Big], \tag{A.1f}$$

where Ξ' parameters are

$$T_{ij}{}' = \left\langle \Psi_i \left| \mathcal{T} \right| \Psi_j \right\rangle, \tag{A.2a}$$

$$V'_{ijkl} = \left\langle \Psi_i\Psi_j \left| \mathcal{V}_{12} \right| \Psi_k\Psi_l \right\rangle, \tag{A.2b}$$

with $\mathcal{T} = -\bigtriangledown^2 - 2/|\mathbf{r}-\mathbf{R}|$, and $\mathcal{V} = 2/|\mathbf{r}-\mathbf{r}'|$. *The single-particle parameters* read

$$\epsilon' = \alpha^2 - 2\alpha - \frac{2}{R} + 2\left(\alpha+\frac{1}{R}\right)e^{-2\alpha R}, \tag{A.3a}$$

$$t' = \alpha^2 e^{-\alpha R}\left(1+\alpha R - \frac{1}{3}\alpha^2R^2\right) - 4\alpha e^{-\alpha R}(1+\alpha R), \tag{A.3b}$$

$$U' = \frac{5}{4}\alpha, \tag{A.3c}$$

$$K' = \frac{2}{R} - \alpha e^{-2\alpha R}\left(\frac{2}{\alpha R} + \frac{3}{2}\alpha R + \frac{1}{3}\alpha^2R^2 + \frac{11}{4}\right), \tag{A.3d}$$

$$V' = \alpha e^{-\alpha R}\left(2\alpha R + \frac{1}{4} + \frac{5}{8\alpha R}\right) - \frac{1}{4}\alpha e^{-3\alpha R}\left(1 + \frac{5}{2\alpha R}\right), \tag{A.3e}$$

$$J' = \alpha e^{-2\alpha R}\left(\frac{5}{4} - \frac{23}{10}\alpha R - \frac{6}{5}\alpha^2 R^2 - \frac{2}{15}\alpha^3 R^3\right) + \frac{12}{5R}\Big(S^2 C_E + S^2 \log(\alpha R) - 2\,S\bar{S}\,\mathrm{Ei}(-2\alpha R) + \bar{S}^2\mathrm{Ei}(-4\alpha R)\Big), \tag{A.3f}$$

where the overlaps are given by

$$S = e^{-\alpha R}\left(1 + \alpha R + \frac{1}{3}\alpha^2 R^2\right), \tag{A.4}$$

$$\bar{S} = e^{\alpha R}\left(1 - \alpha R + \frac{1}{3}\alpha^2 R^2\right). \tag{A.5}$$

C_{E} is so-called Euler constant

$$C_{\mathrm{E}} = \lim_{n\to\infty}\left(\sum_{k=1}^{n}\frac{1}{k} - \log(n)\right) \approx 0.5772, \tag{A.6}$$

and $Ei(x)$ is the exponential integral.

$$Ei(x) = -\int_{-x}^{\infty} e^{-t}t^{-1}\mathrm{d}t. \tag{A.7}$$

Appendix B. Adiabatic-approximation details

For the sake of completeness, we also provide the explicit form of the coupling constants $\xi_i \equiv \mathrm{d}\Xi_i/\mathrm{d}R$. For editorial purposes we calculate first *the single-particle coupling constants* from (A.3*a*). They are

$$\delta\epsilon' = 2R^{-2}e^{-2\alpha R}\Big[e^{2\alpha R} - 1 - 2\,R\alpha\Big(1 + \alpha R\Big)\Big], \tag{B.1a}$$

$$\delta t' = \frac{1}{3}e^{-\alpha R}\alpha^3\,R[12 + \alpha(-5 + \alpha R)], \tag{B.1b}$$

$$\delta U' = 0. \tag{B.1c}$$

The corresponding derivatives of the two-particle parameters are

$$\delta K' = \frac{1}{3}R^{-2}e^{-2\alpha R}\Big[6 - 6e^{2\alpha R} + \alpha R(2 + \alpha R)(6 + \alpha R(3 + 2\alpha R))\Big] \tag{B.1d}$$

$$\delta V' = \frac{1}{8}R^{-2}\Big(e^{-3\,R\alpha}\Big[5 + 15\,R\alpha + 6R^2\alpha^2\Big] - e^{-R\alpha}\Big[5 + 5R\alpha - 14R^2\alpha^2 + 16R^3\alpha^3\Big]\Big) \quad \text{(B.1}e\text{)}$$

$$\begin{aligned}\delta J' = \frac{1}{15R^2}e^{-2\,R\alpha}\Big(&-4C_E\Big[9 + 18R\alpha + 21R^2\alpha^2 + 18R^3\alpha^3 + 9R^4\alpha^4 + 2R^5\alpha^5\Big]\\ &+ R^2\alpha^2\Big[72 + 33R\alpha + 30R^2\alpha^2 + 4R^3\alpha^3\Big] + 4e^{4\,R\alpha}\\ &\times\Big[-9 + 18R\alpha - 21R^2\alpha^2 + 18R^3\alpha^3 - 9R^4\alpha^4 + 2R^5\alpha^5\Big]\mathrm{Ei}\Big(-4R\alpha\Big)\\ &- 24e^{2\,R\alpha}\Big(-3 - R^2\alpha^2 + R^4\alpha^4\Big)\mathrm{Ei}\Big(-2R\alpha\Big) - 36\log(R\alpha)\\ &- 4R\alpha\Big(18 + 21R\alpha + 18R^2\alpha^2 + 9R^3\alpha^3 + 2R^4\alpha^4\Big)\log(R\alpha)\Big)\end{aligned} \quad \text{(B.1}f\text{)}$$

with basis mixing-parameters β and γ (see (3)) changes

$$\delta\beta = \frac{S}{4\big(1 - S^2\big)\beta}\left(\frac{1}{\sqrt{1 - S^2}} + \frac{1}{2\big(1 - S^2\big)}\right)\delta S, \quad \text{(B.2)}$$

$$\delta\gamma = \frac{1}{1 - S^2 + \sqrt{1 - S^2}}\delta S, \quad \text{(B.3)}$$

where S is the overlap (A.4) and δS reads

$$\delta S = -\frac{1}{3}e^{-R\alpha}R\alpha^2\Big(1 + R\alpha\Big). \quad \text{(B.4)}$$

Our final results are

$$\begin{aligned}\xi_\epsilon = 2\frac{\delta\beta}{\beta}\epsilon + \beta^2\Big[&\big(1 + \gamma^2\big)\delta\epsilon' - 2\gamma\delta t'\Big]\\ &+ 2\beta^2\delta\gamma\,[\gamma\epsilon' - t'],\end{aligned} \quad \text{(B.5}a\text{)}$$

$$\begin{aligned}\xi_t = 2\frac{\delta\beta}{\beta}t + \beta^2\Big[&\big(1 + \gamma^2\big)\delta t' - 2\gamma\delta\epsilon'\Big]\\ &+ 2\beta^2\delta\gamma\,[\gamma t' - \epsilon'],\end{aligned} \quad \text{(B.5}b\text{)}$$

$$\begin{aligned}\xi_U = 4\frac{\delta\beta}{\beta}U + \beta^4\Big[&\big(1 + \gamma^4\big)\delta U' + 2\gamma^2\delta K'\\ &- 4\gamma\big(1 + \gamma^2\big)\delta V' + 4\gamma^2\delta J'\Big]\\ &+ 4\beta^4\delta\gamma\Big[\gamma^3U' + \gamma K'\\ &- \big(1 + 3\gamma^2\big)V' + 2\gamma J'\Big],\end{aligned} \quad \text{(B.5}c\text{)}$$

$$\xi_K = 4\frac{\delta\beta}{\beta}K + \beta^4\Big[\,2\gamma^2\delta U' + \left(1+\gamma^4\right)\delta K' - 4\gamma\left(1+\gamma^2\right)\delta V' + 4\gamma^2\delta J'\Big] + 4\beta^4\delta\gamma\Big[\,\gamma U' + \gamma^3 K' - \left(1+3\gamma^2\right)V' + 2\gamma J'\Big], \tag{B.5d}$$

$$\xi_J = 4\frac{\delta\beta}{\beta}J + \beta^4\Big[\,2\gamma^2\delta U' + 2\gamma^2\delta K' - 4\gamma\left(1+\gamma^2\right)\delta V' + \left(1+\gamma^2\right)^2\delta J'\Big] + 4\beta^4\delta\gamma\,[\gamma U' + \gamma K' - \left(1+3\gamma^2\right)V' + \gamma\left(1+\gamma^2\right)J'\Big], \tag{B.5e}$$

$$\xi_V = 4\frac{\delta\beta}{\beta}V - \beta^4\Big[\,\gamma\left(1+\gamma^2\right)\delta U' + \gamma\left(1+\gamma^2\right)\delta K' - \left(1+6\gamma^2+\gamma^4\right)\delta V' + 2\gamma\left(1+\gamma^2\right)\delta J'\Big] - \beta^4\delta\gamma\Big[\left(1+3\gamma^2\right)U' + \left(1+3\gamma^2\right)K' - 4\gamma\left(3+\gamma^2\right)V' + 2\left(1+3\gamma^2\right)J'\Big]. \tag{B.5f}$$

These parameters are displayed versus R in figures 7 and 8.

Appendix C. Zero-point motion with classical electronic interaction

We ask the question of how important it is to include the quantum nature of the electronic interaction in our evaluation of zero-point motion energy. Let us consider, following [9], the energy of the ions as

$$E_{\mathrm{ion}} = \frac{\delta P^2}{2M} + \frac{e^2}{R+\delta R}, \tag{C.1}$$

where δP and δR are the momentum and position uncertainties, M is ion mass and e its charge. By expressing δP by δR via the uncertainty relation $\delta P^2\delta R^2 \geqslant \frac{3}{4}\hbar^2$ we obtain

$$E_{\mathrm{ion}} = \frac{\frac{3}{4}\hbar^2}{2M\delta R^2} + \frac{e^2}{R+\delta R}, \tag{C.2}$$

Table C.1 The values (in atomic units) of the zero-point motion energy and amplitude. The classical electron interaction approximation versus adiabatic approximation.

	$\lvert\delta\mathbf{R}_0\rvert$ (a_0)	E_{ZPM} (Ry)
classical interaction	0.0901816	0.14434
quantum interaction	0.189028	0.024072

which we can minimize with respect to δR. We calculate

$$\delta R_0 \overset{a.u.}{=} \frac{1}{4\sqrt{2}M}\left(a - 1 + \frac{1 - 8\sqrt{2}MR}{a}\right), \tag{C.3}$$

where

$$a \overset{a.u.}{=} \left[-1 + 12\,MR\left(\sqrt{2} - 4\,MR\right) + 2^{15/4}\sqrt{M^3R^3\left(-1 + 9\sqrt{2}MR\right)}\right]^{1/3}. \tag{C.4}$$

We take the mass of the ion $M \overset{a.u.}{\approx} 1836.15267\,m_0$ and the interionic distance $R = R_B = 1.430\,17a_0$. The results are presented in the table C.1.

Appendix D. Inclusion of 2*s* orbitals

We would like to estimate the role of higher orbitals both for more realistic description of H_2 systems and future consideration of other elements. We start by taking the $2s$ Slater-type orbital

$$\Psi^{2s}(\mathbf{r}) \equiv \sqrt{\frac{\alpha_{2s}^5}{3\pi}}\ |\mathbf{r}|\ e^{-\alpha_{2s}|\mathbf{r}|}, \tag{D.1}$$

where α_{2s} is the inverse wave function size. It is obviously non-orthogonal with the $1s$ orbital (1) as we have that

$$S_{on}^{\alpha,\,\alpha_{2s}} \equiv \left\langle \Psi^{1s} \middle| \Psi^{2s} \right\rangle = \frac{8\sqrt{3}\,\alpha^{3/2}\alpha_{2s}^{5/2}}{(\alpha + \alpha_{2s})^4}. \tag{D.2}$$

D.1. On-site orthogonalization

We perform the orthogonalization by introducing realistic orbital functions [36]

$$\chi^{1s}(\mathbf{r}) = \Psi^{1s}(\alpha,\,\mathbf{r}), \tag{D.3}$$

$$\chi^{2s}(\mathbf{r}) = A\Psi^{1s}(\alpha_{2s},\,\mathbf{r}) + B\Psi^{2s}(\alpha_{2s},\,\mathbf{r}), \tag{D.4}$$

where A and B are mixing parameters obtained via orthonormality conditions

$$\left\langle \chi^{1s} \middle| \chi^{2s} \right\rangle = 0,$$
$$\left\langle \chi^{2s} \middle| \chi^{2s} \right\rangle = 1. \tag{D.5}$$

We can solve problem (D.5) analytically and obtain

$$A = -\frac{S_{on}^{\alpha,\,\alpha_{2s}}}{\sqrt{S_{1s}^{\alpha,\,\alpha_{2s}2} - 2S_{1s}^{\alpha,\,\alpha_{2s}} S_{\mathrm{on}}^{\alpha,\,\alpha_{2s}} S_{\mathrm{on}}^{\alpha_{2s},\,\alpha_{2s}} + S_{\mathrm{on}}^{\alpha,\,\alpha_{2s}2}}},$$
$$B = \frac{S_{1s}^{\alpha,\,\alpha_{2s}}}{\sqrt{S_{1s}^{\alpha,\,\alpha_{2s}2} - 2S_{1s}^{\alpha,\,\alpha_{2s}} S_{\mathrm{on}}^{\alpha,\,\alpha_{2s}} S_{\mathrm{on}}^{\alpha_{2s},\,\alpha_{2s}} + S_{\mathrm{on}}^{\alpha,\,\alpha_{2s}2}}}, \tag{D.6}$$

where S_{on} is given by (D.6) and

$$S_{1s}^{\alpha,\,\alpha_{2s}} \equiv \left\langle \Psi^{1s} \middle| \Psi^{1s} \right\rangle = \frac{8(\alpha\alpha_{2s})^{3/2}}{(\alpha + \alpha_{2s})^3}. \tag{D.7}$$

D.2. Intersite orthogonalization

As χ^σ s are orthogonal on-site, one can also introduce intersite orthogonalization. We introduce the following mixing coefficients (2)

$$w_i^\sigma(\mathbf{r}) = \beta^\sigma\left(\chi_i^\sigma(\mathbf{r}) - \gamma^\sigma\chi_j(\mathbf{r})\right), \tag{D.8}$$

where β^σ and γ^σ depend only on the overlap integral $S^\sigma \equiv \langle\chi_1^\sigma|\chi_2^\sigma\rangle$:

$$\beta^\sigma = \frac{1}{\sqrt{2}}\sqrt{\frac{1 + \sqrt{1 - \left(S^\sigma\right)^2}}{1 - \left(S^\sigma\right)^2}} \tag{D.9}$$

$$\gamma^\sigma = \frac{S^\sigma}{1 + \sqrt{1 - \left(S^\sigma\right)^2}}. \tag{D.10}$$

We already have overlap S^{1s} (A.4).

Overlap S^{2s} is only a little bit more complicated

$$\begin{aligned} S^{2s} &= \left\langle \chi_1^{2s} \middle| \chi_2^{2s} \right\rangle = \left\langle A\Psi_1^{1s} + B\Psi_1^{2s} \middle| A\Psi_2^{1s} + B\Psi_2^{2s} \right\rangle \\ &= A^2\left\langle \Psi_1^{1s} \middle| \Psi_2^{1s} \right\rangle + 2\,AB\left\langle \Psi_1^{1s} \middle| \Psi_2^{2s} \right\rangle + B^2\left\langle \Psi_1^{2s} \middle| \Psi_2^{2s} \right\rangle \\ &= A^2 S^{1s,\alpha_{2s}} + 2\,ABS^{1s,2s} + B^2 S^{2s}, \end{aligned} \tag{D.11}$$

where

$$S^{1s,2s} = \frac{e^{\alpha_{2s}(-R)}\left(\alpha_{2s}R\left(\alpha_{2s}R\left(\alpha_{2s}R + 4\right) + 9\right) + 9\right)}{6\sqrt{3}}, \tag{D.12}$$

$$S^{2s} = \frac{1}{45}e^{\alpha_{2s}(-R)}\left(\alpha_{2s}R\left(\alpha_{2s}R\left(\alpha_{2s}R\left(\alpha_{2s}R + 5\right) + 20\right) + 45\right) + 45\right). \tag{D.13}$$

D.3. Single-particle microscopic parameters

Introducing $2s$ orbitals provides us with four new single-particle microscopic parameters

$$\epsilon_{2s} = \left\langle w_i^{2s}(\mathbf{r}) \left| \mathcal{H}_1 \right| w_i^{2s}(\mathbf{r}) \right\rangle, \tag{D.14a}$$

$$t_{2s} = \left\langle w_i^{2s}(\mathbf{r}) \left| \mathcal{H}_1 \right| w_i^{2s}(\mathbf{r}) \right\rangle, \tag{D.14b}$$

$$V_{on} = \left\langle w_i^{1s}(\mathbf{r}) \left| \mathcal{H}_1 \right| w_i^{2s}(\mathbf{r}) \right\rangle, \tag{D.14c}$$

$$V_{inter} = \left\langle w_i^{1s}(\mathbf{r}) \left| \mathcal{H}_1 \right| w_i^{2s}(\mathbf{r}) \right\rangle, \tag{D.14d}$$

where ϵ_{2s} is single-particle energy on the $2s$ orbital, t_{2s} the hopping between $2s$ sites, and V_{on} and V_{inter} are hybridizations on- and inter-site respectively.

Similarly to sections appendix A and B, the exact solution is a function of Slater microscopic parameters

$$\begin{aligned}\epsilon_{2s} = \beta^{2s^2}\Big(A^2\Big(\big(\gamma^2+1\big)\epsilon'_{1s} - 2\gamma t'_{1s}\Big) + 2\,AB\Big(\big(\gamma^2+1\big)V'_{\mathrm{on}} - 2\gamma V'_{\mathrm{inter}}\Big) \\ + B^2\Big(\big(\gamma^2+1\big)\epsilon'_{2s} - 2\gamma t'_{2s}\Big)\Big),\end{aligned} \tag{D.15a}$$

$$\begin{aligned}t_{2s} = \beta^{2s^2}\Big(A^2\Big(\big(\gamma^2+1\big)t'_{1s} - 2\gamma \epsilon'_{1s}\Big) + 2\,AB\Big(\big(\gamma^2+1\big)V'_{\mathrm{inter}} - 2\gamma V'_{\mathrm{on}}\Big) \\ + B^2\Big(\big(\gamma^2+1\big)t'_{2s} - 2\gamma \epsilon'_{2s}\Big)\Big),\end{aligned} \tag{D.15b}$$

$$\begin{aligned}V_{\mathrm{on}} = \beta^{1s}\beta^{2s}\Big(A\Big(\big(\gamma^{1s}\gamma^{2s}+1\big)\epsilon''_{1s} - \big(\gamma^{1s}+\gamma^{2s}\big)t''_{1s}\Big) \\ + B\Big(\big(\gamma^{1s}\gamma^{2s}+1\big)V''_{\mathrm{on}} - \big(\gamma^{1s}+\gamma^{2s}\big)V''_{\mathrm{inter}}\Big)\Big),\end{aligned} \tag{D.15c}$$

$$\begin{aligned}V_{\mathrm{inter}} = \beta^{1s}\beta^{2s}\Big(A\Big(\big(\gamma^{1s}\gamma^{2s}+1\big)t''_{1s} - \big(\gamma^{1s}+\gamma^{2s}\big)\epsilon''_{1s}\Big) \\ + B\Big(\big(\gamma^{1s}\gamma^{2s}+1\big)V''_{\mathrm{inter}} - \big(\gamma^{1s}+\gamma^{2s}\big)V''_{\mathrm{on}}\Big)\Big),\end{aligned} \tag{D.15d}$$

where A and B are found via (D.5), while β^{σ} and γ^{σ} via (D.9). The Slater microscopic parameters can be explicitly written in a form

$$\epsilon'_{1s} = \frac{1}{R}e^{-2\alpha_{2s}R}\Big(2\alpha_{2s}R + e^{2\alpha_{2s}R}\Big(\big(\alpha_{2s}-2\big)\alpha_{2s}R - 2\Big) + 2\Big) \tag{D.16}$$

$$t'_{1s} = -\frac{1}{3}\alpha_{2s}e^{\alpha_{2s}(-R)}\big(\alpha_{2s}\big(R\big(\alpha_{2s}\big(\alpha_{2s}R-3\big)+12\big)-3\big)+12\big), \tag{D.17}$$

$$\begin{aligned}\epsilon'_{2s} = \frac{1}{3R}e^{-2\alpha_{2s}R}\Big(e^{2\alpha_{2s}R}\big(\big(\alpha_{2s}-3\big)\alpha_{2s}R - 6\big) \\ + \alpha_{2s}R\big(2\alpha_{2s}R\big(\alpha_{2s}R+3\big)+9\big)+6\big),\end{aligned} \tag{D.18}$$

$$t'_{2s} = -\frac{1}{45}\alpha_{2s}e^{\alpha_{2s}(-R)}\big(\alpha_{2s}\big(R\big(\alpha_{2s}\big(R\big(\alpha_{2s}R\big(\alpha_{2s}\big(\alpha_{2s}R-5\big)+10\big)+40\big)-15\big)+90\big)-15\big)+90\big), \tag{D.19}$$

$$V'_{on} = \frac{1}{2\sqrt{3}R}e^{-2\alpha_{2s}R}\Big(4\alpha_{2s}^2R^2+8\alpha_{2s}R+e^{2\alpha_{2s}R}\Big(\big(\alpha_{2s}-4\big)\alpha_{2s}R-6\Big)+6\Big), \tag{D.20}$$

$$V'_{inter} = -\frac{1}{6\sqrt{3}}\alpha_{2s}e^{\alpha_{2s}(-R)}\Big(\alpha_{2s}^4R^3-4\alpha_{2s}^3R^2+3\alpha_{2s}^2R(4R-1)+3\alpha_{2s}(8R-1)+24\Big), \tag{D.21}$$

$$\epsilon''_{1s} = \frac{8(\alpha\alpha_{2s})^{3/2}}{R(\alpha+\alpha_{2s})^3}e^{-R(\alpha+\alpha_{2s})}\Big(R(\alpha+\alpha_{2s})+e^{R(\alpha+\alpha_{2s})}\times\big(\big(\alpha-1\big)\alpha_{2s}R+\alpha\big(-R\big)-2\big)+2\Big), \tag{D.22}$$

$$\begin{aligned} t''_{2s} = -\frac{8(\alpha\alpha_{2s})^{3/2}}{R\big(\alpha^2-\alpha_{2s}^2\big)^3}e^{-R(\alpha+\alpha_{2s})}\Big(&e^{\alpha R}\Big(-2\alpha^2\big(\alpha+1\big)\alpha_{2s}\\ &-2\big(\alpha-1\big)\alpha_{2s}^3+\alpha^3\big(\alpha R+2\big)\\ &+\big(\alpha-1\big)\alpha_{2s}^4\big(-R\big)+\alpha\alpha_{2s}^2\Big(\big(\alpha-2\big)\alpha R-2\Big)\Big)\\ &+e^{\alpha_{2s}R}\Big(2\alpha^3\big(\alpha_{2s}-1\big)+2\alpha\alpha_{2s}^2\big(\alpha_{2s}+1\big)\\ &+\alpha^4\big(\alpha_{2s}-1\big)R+\alpha^2\alpha_{2s}\big(2-\big(\alpha_{2s}-2\big)\alpha_{2s}R\big)-\alpha_{2s}^3\big(\alpha_{2s}R+2\big)\Big)\Big), \end{aligned} \tag{D.23}$$

$$V''_{on} = \frac{8\alpha^{3/2}\alpha_{2s}^{5/2}}{\sqrt{3}R(\alpha+\alpha_{2s})^4}e^{-R(\alpha+\alpha_{2s})}\big(R\big(\alpha+\alpha_{2s}\big)\big(R\big(\alpha+\alpha_{2s}\big)+4\big)-e^{R(\alpha+\alpha_{2s})}\big(R\big(\alpha\big(\alpha-2\alpha_{2s}+2\big)+2\alpha_{2s}\big)+6\big)+6\big), \tag{D.24}$$

$$\begin{aligned} V''_{inter} = \frac{8\alpha^{3/2}\alpha_{2s}^{5/2}}{\sqrt{3}R(\alpha-\alpha_{2s})^4(\alpha+\alpha_{2s})^4}e^{-5\alpha R-4\alpha_{2s}R}\Big(&e^{4R(\alpha+\alpha_{2s})}\\ &\times\Big(2\alpha^5+8\alpha^3\alpha_{2s}\big(2\alpha_{2s}-1\big)+2\alpha\alpha_{2s}^3\big(3\alpha_{2s}+4\big)\\ &+\alpha^6R+2\alpha^4\Big(\big(\alpha_{2s}-1\big)\alpha_{2s}R+1\Big)+\alpha^2\alpha_{2s}^2\big(\alpha_{2s}\big(4-3\alpha_{2s}\big)R+4\big)\\ &-2\alpha_{2s}^4\big(\alpha_{2s}R+3\big)\Big)\\ &-e^{5\alpha R+3\alpha_{2s}R}\Big(\big(\alpha-1\big)\alpha_{2s}^6R^2+\alpha^4\Big(\alpha\Big(R\big(\alpha R+2\big)+2\Big)+2\Big)\\ &-4\alpha^3\alpha_{2s}\big(\alpha\big(\alpha+1\big)R+2\big)\Big) \end{aligned}$$

Table D.1 The values of single-particle microscopic parameters without optimization of $2s$ orbitals for $1s$ and $2s$ band ($R = R_B$, $\alpha = \alpha_B$, $\alpha_{2s} = \alpha_B/2$). Note that the last column describes atomic limit, where $\alpha \to 1$, $\alpha_{2s} \to 0.5$. We can observe that the model fulfills requirements, as the Wannier function w_i^{2s} approaches the exact solution of Hydrogen atom.

	Equilibrium system			Atomic limit
microscopic parameter Ξ	$\Xi^{2s}(Ry)$	$\Xi^{1s}(Ry)$	Ξ^{2s}/Ξ^{1s}	$\Xi^{2s}(Ry)$
ϵ	−0.518585	−1.75079	29.62%	−0.25
t	−0.292465	−0.727647	40.19%	0
V_{on}	0.0773174			0
V_{inter}	−0.110457			0

$$+\alpha^2\alpha_{2s}^2\Big(\alpha\Big(R\Big(\big(\alpha-3\big)\alpha R-4\Big)+16\Big)+4\Big)+4\big(\alpha-1\big)\alpha_{2s}^5 R$$
$$+\alpha_{2s}^4\Big(\alpha\Big(R\Big(\alpha\big(3-2\alpha\big)R+2\Big)+6\Big)-6\Big)+8\alpha\alpha_{2s}^3\big(\alpha R+1\big)\Big)\Big). \tag{D.25}$$

One can obtain the exact values for the optimal inter-ionic distance $R = R_B = 1.430\,42$ and $\alpha = \alpha_B = 1.193\,78$. The results, together with comparison to the one-orbital case, are listed in table D.1. Note that the new estimates are carried out for the optimal bond length and the inverse wave-functions size for the case of $1s$ functions only ($R = R_B = 1.430\,42$ and $\alpha = \alpha_B = 1.193\,78$, respectively).

References

[1] Spalek J, Oleś A M and Chao K A 1981 *Phys. Stat. Sol.* (b) **108** 329
[2] Penson K A and Kolb M 1986 *Phys. Rev.* B **33** 1663
[3] de Boer J and Schadschneider A 1995 *Phys. Rev. Lett.* **75** 4298
[4] Iglesias J R, Gusmão M A, Acquarone M, Romano A and Noce C 1997 *Physica* B **230–232** 1047
[5] Schumann R 2002 *Ann. Phys. (Leipzig)* **11** 49
[6] Schumann R 2008 *Ann. Phys. (Leipzig)* **17** 221
[7] Acquarone M, Iglesias J R, Gusmão M A, Noce C and Romano A 1997 *Il Nuovo Cimento* D **19** 1345
[8] Matlak M, Grabiec B and Krawiec S 2007 *Acta Phys. Polon.* A **112** 537
[9] Spałek J, Podsiadły R, Wójcik W and Rycerz A 2000 *Phys. Rev.* B **61** 15676
[10] For review see: Spałek J, Görlich E M, Rycerz A and Zahorbeński R 2007 *J. Phys.: Condens. Matter* **19** 255212
[11] Oleś A M, Spałek J and Chao K A 1979 *Physica* A **97** 565
[12] Spałek J, Oleś A M and Chao K A 1979 *Physica* A **97** 552
[13] Kadzielawa A P, Spałek J, Kurzyk J and Wójcik W 2013 *Eur. Phys. J.* B **86** 252
[14] Weir S T, Mitchell A C and Nellis W J 1996 *Phys. Rev. Lett.* **76** 1860–3
[15] Sorella S and Capriotti L 2010 *J. Chem. Phys.* **133** 234111
[16] Ashcroft N W 2000 *J. Phys.: Condens. Matter* **12** A129
[17] Shibata K, Ohashi T, Ogawa T and Kodama R 2010 *Phys. Rev.* B **82** 195123
[18] McMahon J M and Ceperley D M 2011 *Phys. Rev. Lett.* **106** 165302
[19] Naumov I I, Cohen R E and Hemley R J 2013 *Phys. Rev.* B **88** 045125
[20] Slater J C 1963 *Quantum Theory of Molecules and Solids* vol 1 (New York: McGraw-Hill)

[21] Kołos W and Wolniewicz L 1968 *J. Chem. Phys.* **49** 404
Kołos W and Wolniewicz L 1964 *J. Chem. Phys.* **41** 3663
[22] Szabo A and Ostlund N S 1989 *Modern Quantum Chemistry* (Mineola, New York: Dover Publications)
[23] Acquarone M and Noce C 1999 *Int. J. Mod. Phys.* B **13** 3331
[24] Spaek J 2008 *Condens. Matter Phys.* **11** 455
[25] Su W P, Schrieffer J R and Heeger A J 1980 *Phys. Rev.* B **22** 2099–111
[26] Holstein T 1959 *Ann. Phys., NY* **8** 325–42
[27] Rycerz A 2003 Physical properties and quantum phase transitions in strongly correlated electron systems from a combined exact diagonalization–*ab initio* approach *PhD Thesis* Jagiellonian University
[28] Kochanski E, Roos B, Siegbahn P and Wood M 1973 *Theoret. Chim. Acta (Berl.)* **32** 151
[29] Hobza P, Zahradnĺk R and Čársky P 1979 *Theoret. Chim. Acta (Berl.)* **53** 1–7
[30] Martínez J I, Isla M and Alonso J A 2007 *Eur. Phys. J.* D **43** 61–64
[31] Ceperley D M and Alder B J 1980 *Phys. Rev. Lett.* **45** 566
[32] Traynor C A, Anderson J B and Boghosian B M 1991 *J. Chem. Phys.* **94** 3657
[33] Azadi S, Monserrat B, Foulkes W M C and Needs R J 2014 *Phys. Rev. Lett.* **112** 165501
[34] Lee J and Haule K 2014 arXiv:1403.2474
[35] Dickenson G D, Niu M L, Salumbides E J, Komasa J, Eikema K S E, Pachucki K and Ubachs W 2013 *Phys. Rev. Lett.* **110** 193601
[36] Calderini D, Cavalli S, Coletti C, Grossi G and Aquilanti V 2012 *J. Chem. Sci.* **124** 187–92